A QUANTITATIVE ULTRASOUND-BASED METHOD AND DEVICE FOR RELIABLY GUIDING PATHOLOGISTS TO METASTATIC REGIONS OF DISSECTED LYMPH NODES

Alain Coron,[1,2] *Jonathan Mamou,*[3] *Emi Saegusa-Beecroft,*[4] *Michael L. Oelze,*[5] *Tadashi Yamaguchi,*[6] *Masaki Hata,*[4] *Junji Machi,*[4] *Eugene Yanagihara,*[4] *Pascal Laugier,*[1,2] *Ernest J. Feleppa*[3]

[1] UPMC Univ Paris 06, UMR7623, Paris France
[2] CNRS, UMR7623 LIP, Paris, France
[3] Frederic L. Lizzi Center for Biomedical Engineering, Riverside Research, New York, NY
[4] University of Hawaii and Kuakini Medical Center, Honolulu, HI
[5] Bioacoustic Research Laboratory, Department of Electrical and Computer Engineering, University of Illinois, Urbana, IL
[6] Research Center for Frontier Medical Engineering, Chiba University, Chiba, Japan

ABSTRACT

Our group is developing a method based on 3D high-frequency ultrasound (HFU) and 3D quantitative ultrasound (QUS) to help pathologists detect micrometastases in freshly-excised lymph nodes of patients with histologically-proven primary cancer. From a signal and image processing perspective, we report on our efforts to acquire and classify lymph-node tissue based on 3D QUS parameter estimates. We evaluated classifier performance against gold-standard histology. Using our database of 134 abdominal cancer-free nodes and 26 fully cancerous abdominal nodes, a conservative threshold gave a sensitivity and specificity of 99.3% and 73.1%, respectively. We also constructed a 3D cancer-likelihood map of a partially metastatic lymph node and compared that map with histology. This representation potentially can be useful for guiding pathologists to suspicious regions requiring histological evaluation.

Index Terms— metastatic cancer, lymph nodes, quantitative ultrasound, high-frequency ultrasound, histology, segmentation, registration

1. INTRODUCTION

For many patients with histologically-proven primary cancer, the current standard of care requires at least a formal dissection of 10 to 30 lymph nodes and a time-consuming postoperative complete histologic preparation, sectioning and evaluation to detect possible metastases. Nodal status is crucial for prognosis and treatment planning. However, current histopathology standards may miss clinically significant micrometastases ranging in size from 0.2 to 2 mm because two evaluated consecutive histological sections are usually at least 2 mm apart. In many medical centers, nodes are examined only in a single central plane. Evaluating additional sections generally would not be clinically practical.

Quantitative ultrasound (QUS), which estimates quantitative parameters from ultrasound data, has proven to be sensitive to tissue microstructure [1]. High-frequency ultrasound (HFU, > 15 MHz) has a spatial resolution on the order of 100 μm or better, and allows fast non-destructive 3D characterization of tissues. Our group has investigated 3D high-frequency QUS methods to reliably determine the presence or absence of metastases in freshly-excised lymph nodes of cancer patients [2, 3]. Our novel QUS methods eventually could be used to design a new device to guide pathologists to suspicious regions for definitive histological evaluation. To accomplish this aim, QUS parameters are estimated in 3D and compared to 3D histological representations of the lymph nodes based on a non-standard, fine, step-sectioning procedure. In this paper, we describe our methodology from an image-processing viewpoint and provide up-to-date results and perspectives.

2. METHODS

To develop a QUS processing method and validate the method against the gold-standard histology, our approach involves four major tasks: 1) HFU data acquisition and QUS processing, 2) non-standard histology evaluation and 3D histology reconstruction, 3) QUS classification and classifier performance evaluation, and 4) QUS and histology visualization. Fig. 1 summarizes our approach and subsequent sections detail the methods.

2.1. Ultrasound acquisition and QUS processing

2.1.1. HFU acquisition

Patients who had histologically-proven colorectal, gastric, or breast cancer and who were scheduled for surgical resection were recruited at the Kuakini Medical Center (KMC) in Honolulu, HI, and gave written informed consent as required by cognizant Review Boards.

At the time of surgery, lymph nodes were dissected according to the standard medical procedures applicable for each case. In the case of breast-cancer surgery, sentinal-node procedures were employed for several patients.

Each freshly-excised lymph node was manually defatted by dissection and scanned in a saline bath with a single-element ultrasound transducer (PI30-2-R0.50IN, Olympus NDT, Waltham, MA, USA). The transducer had a center frequency of 25.6 MHz, an aperture of 6.1 mm, and a focal length of 12.2 mm; its -6-dB bandwidth extended from 16.4 to 33.6 MHz. A 3D scan of each lymph node was obtained by scanning adjacent lines and planes every 25 μm over the entire lymph node with our custom HFU system. At all times, the transducer axis was parallel to the z-axis of the (x, y, z) HFU coordinate system. Resulting ultrasound images had axial and lateral

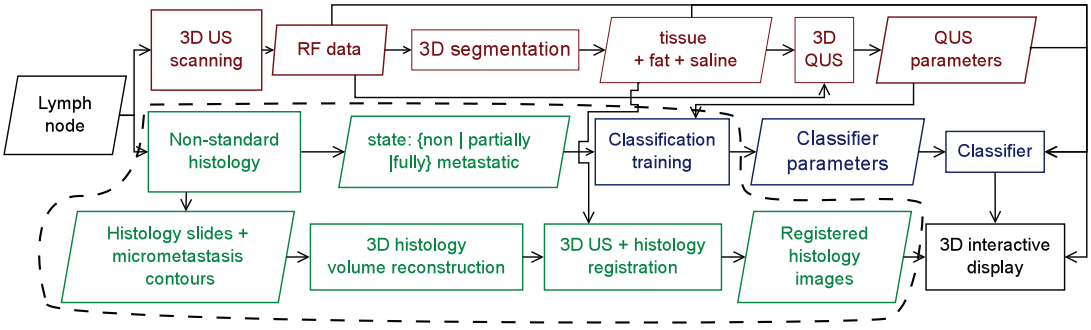

Fig. 1. Main processing steps: US acquisition and QUS parameter estimation in red, non-standard histology evaluation and 3D reconstruction in green, QUS classification and performance evaluation in blue. Elements surrounded by a dashed line are essential to set up and estimate the performance of the QUS estimate, but will not be included in the proposed pathology device.

resolutions of 85 and 116 μm, respectively. Radio-frequency (RF) echo signals were digitized with a precision of 8-bits at a sampling rate of 400 MS/s.

2.1.2. 3D segmentation

Segmenting tissue from fat and saline is essential to restrict QUS processing to lymph-node tissue. Segmentation results are also used to correct QUS parameters for attenuation through remaining perinodal fat tissue and in the node tissue.

First, the envelope of the 3D RF dataset was computed and downsampled by a factor of 8 using Mallat's pyramidal algorithm to compute the discrete wavelet transform approximation coefficients a_e. (The mother wavelet was the symmetric biorthogonal cubic spline wavelet [4].)

Second, a semi-automatic segmentation based on a pseudo maximum-likelihood region was implemented [5]. Segmentation took advantage of the fact that, at the focus, saline is less echogenic than tissue, and tissue is less echogenic than fat. Thus, two thresholds T_{ST} and T_{TF} were estimated at the focus to classify regions as saline ($20\log_{10}|\bar{a_e}| < T_{ST}$), tissue ($T_{ST} \leq 20\log_{10}|\bar{a_e}| < T_{TF}$) or fat ($T_{TF} \leq 20\log_{10}|\bar{a_e}|$). To take into account the local ultrasound field properties at depth d in the segmentation, a term $C(d)$ was added to T_{ST} and T_{TF}. $C(d)$ was set to the maximum of the calibration curve at depth d. The calibration curve was obtained from the echoes off a weak reflector at normal incidence placed at a range of depths in the field of the ultrasound source. The original regions were delimited by a watershed after morphological filtering of $20\log_{10}|a_e|$.

2.1.3. 3D QUS estimation

QUS parameters were estimated in overlapping 3D cylindrical analysis regions (AR) having a 1-mm diameter and a 1-mm length along the transducer axis. The parameters were computed only if all the RF samples in the AR were determined by the 3D segmentation to be lymph-node tissue and if the SNR was higher than a preset threshold. In total, thirteen QUS parameters were estimated. Four were extracted from two different fits of the normalized and attenuation-compensated local power spectrum of the backscattered RF. The first fit was a straight line [6] and the second derived from a Gaussian scattering model [7]. This second model was used to estimate the effective scatterer size D, and the acoustic concentration CQ^2. Four other parameters were estimated by considering the probability density function of the envelope to be a Nakagami [8] or homodyned-K

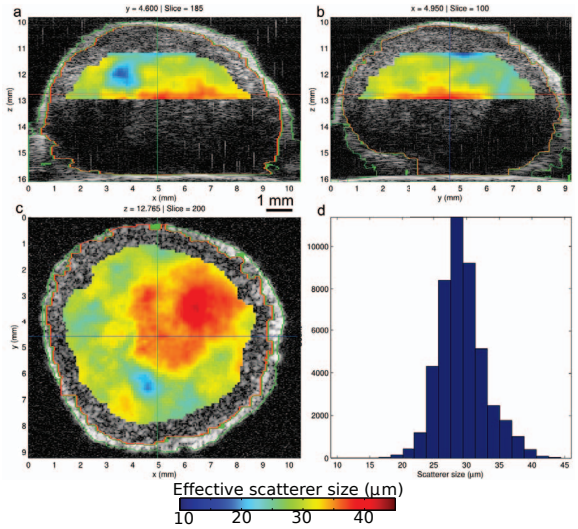

Fig. 2. (a)–(c) Ultrasound images generated from RF signals and color-encoded effective scatterer size in three orthogonal cross-sections of a lymph node. Segmented tissue and fat regions are highlighted in red and green. For this large node, the automatic segmentation was manually corrected. (d) histogram of the effective scatterer size.

distribution [9]. These distributions express the envelope statistics of ultrasound data. Finally, the remaining five easy-to-compute parameters were obtained using a Rayleigh-crafted distribution function plot [10]. They quantify the degree to which the AR statistics are consistent with a Rayleigh distribution.

2.2. Non-standard histology

Following ultrasound scanning, the lymph node was inked to permit the recovery of the histologic data correctly oriented with respect to the ultrasound data. The surface of the node proximal to the transducer was inked in red; the distal surface was inked in blue; and the end facing the positive x direction was inked in black. Therefore, the red-blue junction defined a plane perpendicular to the transducer axis. The node was cut in half longitudinally along the red-blue junction. Then the two half nodes were fixed and embedded in paraffin with the flat-cut surface downward.

The inked, fixed, and embedded node underwent a standard histology procedure using non-standard finely spaced step sections and standard H&E stained thin sections. Thin sections were obtained every 65 μm for nodes smaller than 5 mm and at 115 μm for larger nodes, which is much finer than current standard of care. Stained and mounted thin sections were digitized with a high-throughput slide scanner (NanoZoomer, Hamamatsu) with a resolution of 0.46 μm.

The resulting images I_n contained one slice from each of the two (red and blue) opposite lymph-node halves. However, the last images might reduce to a set of unique sections because nodes were not symmetric. Furthermore, sections might be incomplete or torn, especially on those derived from the initial central cut. Tissue shrinkage was inherent in histologic preparation, and on a few slides, large sections occasionally touched each other.

A pathologist examined each node and classified it as non-metastatic, partially metastatic, or fully metastatic, and in particular, the pathologist demarcated the boundary of metastatic regions with a green polyline.

One slide also was digitized with two additional pairs of (black,blue) and (black,red) dots to indicate for each half node the positive x-axis direction. The pathologist added those dots after careful examination of the color of the lymph-node boundaries. This image was named T3.

2.3. 3D histology volume reconstruction and registration with US data

A 3D histology volume was automatically assembled from the stack of histology images [11]. To achieve this reconstruction, the two slices on each slide were isolated with a parametric shape model incorporating two non-overlapping ellipses, $\mathcal{E}_1$ and $\mathcal{E}_2$, that covered as much tissue as possible and as little background as possible. Pixels were classified as tissue or background by thresholding the saturation channel. Then, a cost function $\mathcal{C}(\mathcal{E}_1, \mathcal{E}_2)$ was designed as a linear combination of four terms; the combination was minimized using an iterative gradient-descent method. Those four terms are $\mathcal{C}_T$ and $\mathcal{C}_B$, the cost terms associated with the tissue and the background, $\mathcal{C}_I$, a term to penalize ellipse intersection, and $\mathcal{C}_\varepsilon$, a term to penalize flat ellipses.

The location of each section was extracted from the estimated ellipses $\mathcal{E}_1$ and $\mathcal{E}_2$,. Then each slide (image with one slice of each half node) limited to a bounding box of the ellipses was rigidly registered with the next slide with elastix [12]. The mutual information of the saturation component of the two images served as the similarity measure.

The set of bisectors of the points $P_1 \in \mathcal{E}_1$ and $P_2 \in \mathcal{E}_2$ that minimized the Euclidian distance between the two ellipses, was used to separate the halves. By using the bisectors and combining the set of rigid transforms estimated previously, the sections of each halves were realigned and separated.

The orientation of the HFU data set was recovered from the detected pairs of dots on T3 and the 3D histologic volume was aligned with the 3D HFU data. The histologic volume was scaled along the z-direction because of lymph-node shrinkage, partly during US scanning but mostly during histologic preparation.

2.4. Classification

Lymph nodes with a cancer volume of at least 65% of the node volume and entirely cancer-free nodes were used to develop and evaluate classifiers based on linear-discriminant analysis. Each individual QUS parameter estimate, as well as various linear combinations of them were assessed as potential two-class classifiers. The performance of each combination of QUS estimates was determined by producing ROC curves depicting the tradeoff between sensitivity and specificity and the overall classification performance. The area-under-the-curve (AUC) values were computed. Additionally, sensitivity and specificity values obtained using a clinically-conservative operating point (i.e., at high sensitivity) were computed.

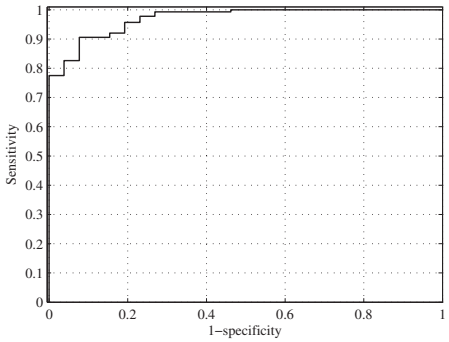

Fig. 3. ROC curve computed with 160 gastrointestinal lymph nodes. 26 of them were fully metastatic.

2.5. 3D interactive display

For this project, highly effective visualization software termed LymphExplorer was developed and used to interactively examine the US image data in 3D by simultaneously displaying three perpendicular cross-sectional views as well as the QUS parameters, the histologic volume and the automatic segmentation, which can be manually corrected. Conventional ultrasound images (Figs. 2a–c) of a large and partially-metastatic colorectal lymph node are shown in gray scale, and segmentation results are outlined in green (fat tissue) and red (lymph-node tissue). Figs. 2a–c also show the effective scatterer size. The value estimated for each AR is color-coded and displayed at the center of the AR. (On this large node, the SNR was too low to compute QUS parameters in the distal bottom half of the node.)

3. RESULTS AND PROTOTYPE DEVICE

We processed 160 lymph nodes from 87 abdominal-cancer patients. Among them, 26 were fully cancerous (i.e., at least 65% of the volume was cancerous). Fig. 3 shows the ROC curve of the optimal linear classifier, which combined 7 of the 13 QUS parameters. The AUC was 0.974 ± 0.011 and (0.952, 0.997) was the 95% confidence interval. Sensitivity and specificity obtained using a clinically-conservative operating point were 99.3% and 73.1%, respectively. So the classification performance was excellent for gastrointestinal-cancer nodes. Slightly lower results were obtained with 94 breast-cancer lymph nodes (79 entirely negative, 15 positive) of 55 cancer patients and an optimal linear classifier which combined 4 of 13 QUS parameters: the AUC was 0.889 ± 0.046. Sensitivity and specificity were 93.3% and 67.1% using a clinically-conservative operating point.

The 3D automatic histology reconstruction was visually quite satisfactory on most of the lymph nodes. Considering the size of the AR, 3D US and histology registration was sufficient and provided additional insights into the method. Figs. 4a–c display a 3D binary image map of the regions having a cancer likelihood lower than 50%

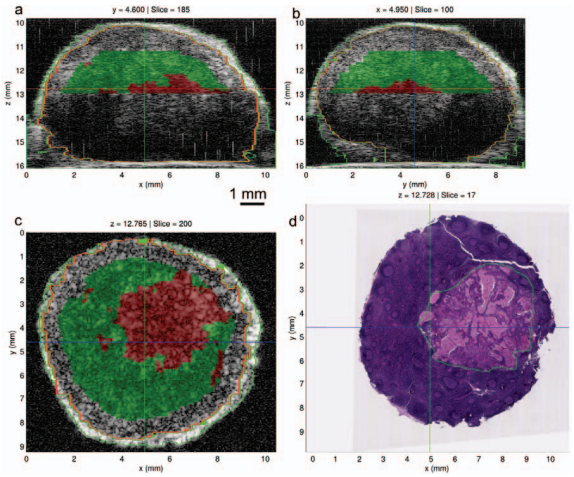

Fig. 4. Partially-metastatic lymph node from colon cancer patient. (a)–(c) regions with cancer likelihood lower than 50% in green, and higher than 50% in red. (d) matched histology

in green and higher than 50% in red. Fig. 4d presents one plane of the reconstructed 3D histologic volume at the same depth as the US plane of Fig. 4c. In this partially-metastatic node, the regions demarcated by the pathologist as cancerous on the histology image are in good agreement with the QUS cancer-likelihood map. This kind of 3D binary map could be a simple and meaningful representation to guide the pathologist to suspicious regions warranting close histological examination.

At the present time, our laboratory research device consists of a 3D HFU scanner and an off-the-shelf computer devoted to the estimation of cancer regions. It displays the segmentation, the QUS parameters, the registered histology and the cancer-likelihood map in an interactive display of 3D information.

A future clinical device will not display elements surrounded by a dashed line in Figure 1, so the histology panel will be removed from our LymphExplorer software. Currently, segmentation of the US images needs human intervention, especially for large nodes. Therefore, segmentation must be improved, and we expect to update it with a more-effective, time-saving, 3D automatic segmentation. In addition, we will optimize data acquisition and processing by increasing the scan-vector spacing moderately and determining what AR dimensions provide the best tradeoff between spatial resolution, node coverage, and statistical stability of QUS estimates

4. CONCLUSIONS

More than 250 lymph nodes have been processed to date with the described high-frequency 3D US scanning and QUS processing methodology. Outstanding classification results were obtained on abdominal lymph nodes of colorectal- and gastric-cancer patients, and excellent classification results were achieved on more-complex axillary nodes of breast-cancer patients. Improvements in data acquisition, segmentation, and QUS analysis and display methods are planned, e.g., to expedite processing and better take into account lymph-node shrinkage during scanning and histologic preparation.

Figure 4 suggests that this new representation of US data may offer a valuable means of guiding pathologists to suspicious regions of lymph nodes that warrant histological examination. Because these methods allow rapid reliable ultrasonic interrogation of the entire node volume, they can reduce the chance of overlooking small, but clinically significant micrometastases.

5. ACKNOWLEDGEMENTS

This research was supported in part by NIH Grant CA100183, the Riverside Research Biomedical Engineering Research Fund, and CNRS.

6. REFERENCES

[1] F L Lizzi, M Ostromogilsky, E J Feleppa, M C Rorke, and M M Yaremko, "Relationship of ultrasonic spectral parameters to features of tissue microstructure.," *IEEE Trans. Ultrason., Ferroelectr., Freq. Control*, vol. 34, no. 3, pp. 319–29, Jan. 1987.

[2] J Mamou, A Coron, M L Oelze, E Saegusa-Beecroft, M Hata, P Lee, J Machi, E Yanagihara, P Laugier, and E J Feleppa, "Three-dimensional high-frequency backscatter and envelope quantification of cancerous human lymph nodes.," *Ultrasound Med. Biol.*, vol. 37, no. 3, pp. 345–57, Mar. 2011.

[3] J Mamou, A Coron, M Hata, J Machi, E Yanagihara, P Laugier, and E J Feleppa, "Three-dimensional high-frequency characterization of cancerous lymph nodes.," *Ultrasound Med. Biol.*, vol. 36, no. 3, pp. 361–75, Mar. 2010.

[4] S Mallat, *A Wavelet Tour of Signal Processing*, Academic Press, 1999.

[5] A Coron, J Mamou, M Hata, J Machi, E Yanagihara, P Laugier, and E J Feleppa, "Three-dimensional segmentation of high-frequency ultrasound echo signals from dissected lymph nodes," in *IEEE Int. Ultrason. Symp.*, 2008, pp. 1370–1373.

[6] F L Lizzi, M Greenebaum, E J Feleppa, M Elbaum, and D J Coleman, "Theoretical framework for spectrum analysis in ultrasonic tissue characterization.," *J. Acoust. Soc. Am.*, vol. 73, no. 4, pp. 1366–73, Apr. 1983.

[7] M F Insana, R F Wagner, D G Brown, and T J Hall, "Describing small-scale structure in random media using pulse-echo ultrasound.," *J. Acoust. Soc. Am.*, vol. 87, no. 1, pp. 179–92, Jan. 1990.

[8] P M Shankar, "A general statistical model for ultrasonic backscattering from tissues," *IEEE Trans. Ultrason., Ferroelectr., Freq. Control*, vol. 47, no. 3, pp. 727–736, 2000.

[9] D P Hruska and M L Oelze, "Improved parameter estimates based on the homodyned K distribution.," *IEEE Trans. Ultrason., Ferroelectr., Freq. Control*, vol. 56, no. 11, pp. 2471–81, Nov. 2009.

[10] T Yamaguchi and H Hachiya, "Proposal of a parametric imaging method for quantitative diagnosis of liver fibrosis," *J. Med Ultrasonics*, vol. 37, no. 4, pp. 155–166, July 2010.

[11] A Coron, J Mamou, E Saegusa-Beecroft, M Hata, P Lee, J Machi, E Yanagihara, P Laugier, and E J Feleppa, "Assembling 3D histology volumes from sections of cancerous lymph nodes to match 3D high-frequency quantitative ultrasound images," in *IEEE Int. Ultrason. Symp.*, 2010, pp. 2368–2371.

[12] S Klein, M Staring, K Murphy, M A Viergever, and J P W Pluim, "Elastix: a Toolbox for Intensity-Based Medical Image Registration.," *IEEE Trans. Med. Imag.*, vol. 29, no. 1, pp. 196–205, Jan. 2010.